PHYSICAL REVIEW D **86,** 123010 (2012)

Multidetector $\mathcal{F}$-statistic metric for short-duration nonprecessing inspiral gravitational-wave signals

Drew Keppel*

Albert-Einstein-Institut, Max-Planck-Institut für Gravitationsphysik, D-30167 Hannover, Germany and Leibniz Universität Hannover, D-30167 Hannover, Germany

(Received 27 August 2012; published 17 December 2012)

We derive explicit expressions for the multidetector $\mathcal{F}$-statistic metric applied to short-duration nonprecessing inspiral signals. This is required for template bank production associated with coherent searches for short-duration nonprecessing inspiral signals in gravitational-wave data from a network of detectors. We compare the metric's performance with explicit overlap calculations for all relevant dimensions of parameter space and find the metric accurately predicts the loss of detection statistic above overlaps of 95%. We also show the effect that neglecting the variations of the detector response functions has on the metric.

DOI: 10.1103/PhysRevD.86.123010 PACS numbers: 95.75.Pq, 95.55.Ym, 04.25.dg

I. INTRODUCTION

Inspiral signals are thought to be the most promising source of gravitational waves (GWs) for second generation GW detectors. Depending on the rate of merger events, the Advanced LIGO, Advanced Virgo GW detector network operating at design sensitivity will be able to detect between 0.4 and 400 binary neutron star coalescences per year [1]. Underlying these numbers there is an assumed threshold on the network signal-to-noise ratio (SNR) at which a signal is ''detectable'' (i.e., has a false alarm probability below some established value). It has been shown that, among the different matched-filter-based search strategies, coherent templated searches for these signals can reduce the false alarm rate for the same network SNR compared to coincident templated searches [2–5]. Thus it is attractive to prepare coherent searches for when the advanced detectors come online in order to maximize the number of detected events.

The $\mathcal{F}$-statistic was originally derived as a single-detector detection statistic associated with searching GW data for signals from rotating neutron stars [6], and was extended to multiple-detector analysis in [4]. However, it is equally applicable to coherent searches for GW signals from inspiraling compact objects [2–5], due to the physical similarity of the two emitting systems. The signals from both types of systems can be modeled as GW emission from a rotating quadrupole moment. Both signals can be characterized by four *extrinsic* parameters that affect the amplitude, polarization, and phase offset of the waveform, an extrinsic parameter that sets a reference time for the signal, and *intrinsic* parameters that affect the phase and amplitude evolution of the waveform.

In performing templated matched-filter searches for GWs, one is always faced with the question, ''what template waveforms should the data be filtered against?'' With regards to searches for inspiral signals in single detector GW data, this question has been investigated within a geometric formalism. Specifically, a distance measure can be defined on the parameter space based on the ''mismatch'' between waveforms from different parameter space points [7]. This was initially derived for the two-dimensional mass space for stationary phase approximation (SPA) inspiral waveforms expanded to Newtonian order in the amplitude and 1.0 post-Newtonian (PN) order in the phase, where the effects of the objects' spins were neglected. This has been extended to 3.5 PN order for the ''nonspinning'' contributions to the phase [8,9]. In addition, a higher-dimensional metric has been obtained that includes the ''spin'' contributions to the phase, up to 2.0 PN order, for the case where the objects' spins are aligned with the orbital angular momentum [10].

There have been several pieces of work that have been closely related to deriving the multidetector $\mathcal{F}$-statistic metric for short-duration nonprecessing inspiral signals. The first was the derivation of the mismatch metric for coherent searches of short-duration nonprecessing inspiral signals based purely on the Newtonian order inspiral phase model [11] and built on the formalism of [2,7], which was later extended to cover the phase expanded at 2.5 PN order [12]. Another was the derivation of the multidetector $\mathcal{F}$-statistic metric for rotating neutron stars [13]. In addition, there was the computation of the Fisher matrix for the network SNR of known and unknown waveforms of short and long duration, focusing on obtaining explicit expressions for the angular resolution of a GW detector network [14]. Finally, the most closely related work showed parameter recovery accuracies based on the Fisher matrix applied to inspiral and inspiral-merger-ringdown waveforms observed by detector networks [15], although the derivation of the Fisher matrix was not presented. There has been no equivalent published derivation of the multidetector $\mathcal{F}$-statistic metric for short-duration nonprecessing inspiral signals including both the amplitude model, the phase model, and the directional derivatives effects of detector responses. This is what we derive here to 3.5 PN order in the inspiral phase. This metric is required

*drew.keppel@ligo.org

for determining how to arrange templates that would cover the four-dimensional sky location and mass space of a coherent search.

Previous coherent searches for short-duration nonprecessing inspiral signals have been based on one of three methods. They have either relied on the sky position to be known precisely [16] or known to some degree and tiled by detector triangulation arguments [17]. These have both done a templated search on the mass parameter space in an *ad hoc* way based on mass space coverings associated with a single detector [5]. A third approach has been hierarchical [18], relying on coincident searches of single detector data with their associated mass space coverings to decide what points in the mass space are followed up coherently. The metric derived here could be used as the starting point for determining separately a template covering of the sky as well as the mass space covering for a template bank associated with a coherent search.

Following the formalism laid out for computing the multidetector $\mathcal{F}$-statistic in Refs. [13,19], this work is organized as follows: Sec. II identifies the form of the GW signal from rotating nonprecessing quadrupole moments as seen in a GW network, Sec. III summarizes the formulation of the multidetector $\mathcal{F}$-statistic, Sec. IV outlines the approximations appropriate when applied to short-duration (i.e., much less than one day) nonprecessing inspiral signals, Sec. V derives the metric for the coherent multidetector $\mathcal{F}$-statistic for short-duration nonprecessing inspiral signals, and Sec. VI shows tests of this metric.

II. OBSERVED GW SIGNAL FROM ROTATING NONPRECESSING QUADRUPOLE MOMENTS

To start with, let us identify the parameters that will affect how a generic GW signal from a rotating, nonprecessing quadrupole moment is observed by a GW detector. These parameters can be separated into two classes, intrinsic parameters, which affect the time evolution of the waveform and we will elaborate further on this in Sec. IV, and extrinsic parameters, which affect the polarization, amplitude, and the phase and time offsets. The extrinsic parameters can be further subdivided into two classes, those that can be measured analytically within the matched-filtering process, and those that must be searched over by separate filters. As we will see, the extrinsic parameters that can be measured analytically are the extrinsic amplitude h_0, the inclination angle ι between the line of sight and the total angular momentum of the emitting system, the reference phase ϕ_0, and the polarization angle ψ, which is a rotation between the radiation frame of the GW and the frame of the detector about the direction of propagation $-\hat{n}$.

With those definitions of the extrinsic parameters, we give a signal model that describes how a generic GW signal from a rotating, nonprecessing quadrupole moment will be observed by a detector. A generic propagating GW signal of this form can be described in terms of two polarizations in general relativity,

$$\mathrm{h} := h_+ - ih_\times, \tag{1}$$

where the h_+ and $h_\times$ waveforms are out of phase by 90°. Thus, these waveforms can be written in terms of the intrinsic waveforms $h_c(t)$ and $h_s(t)$ as

$$\mathrm{h} = \hat{A}_+ h_c(t) - i\hat{A}_\times h_s(t). \tag{2}$$

The intrinsic waveforms can be further decomposed into an amplitude piece $\mathsf{A}(t)$ and phase piece $\phi(t)$,

$$\begin{aligned} h_c(t) &:= \mathsf{A}(t)\cos[\phi(t) + \phi_0], \\ h_s(t) &:= \mathsf{A}(t)\sin[\phi(y) + \phi_0], \end{aligned} \tag{3}$$

where $\mathsf{A}(t)$ and $\phi(t)$ will depend on the details of the emitting system. The polarization amplitudes associated with the different polarization waveforms are functions of the extrinsic amplitude h_0 and the inclination angle ι,

$$\hat{A}_+ := \frac{h_0}{2}(1 + \cos^2\iota), \qquad \hat{A}_\times := h_0\cos\iota. \tag{4}$$

The waveform as seen by detector Y can be obtained by taking the real part of this complex waveform projected onto the complex detector response $\mathrm{F}^Y := F^Y_+ + iF^Y_\times$,

$$s^Y(t) = \Re(\mathrm{h}\,\mathrm{F}^Y e^{-i2\psi}), \tag{5}$$

where we give explicit expressions for F^Y_+ and $F^Y_\times$ later in this section. Expanding h, F, and the phase terms of cosine and sine waveforms of (5), we find

$$\begin{aligned} s^Y(t) = {} & (\hat{A}_+\cos\phi_0\cos2\psi - \hat{A}_\times\sin\phi_0\sin2\psi)F^Y_+(t)h^Y_c(t) \\ & + (\hat{A}_+\cos\phi_0\sin2\psi + \hat{A}_\times\sin\phi_0\cos2\psi)F^Y_\times(t)h^Y_c(t) \\ & + (-\hat{A}_+\sin\phi_0\cos2\psi - \hat{A}_\times\cos\phi_0\sin2\psi)F^Y_+(t)h^Y_s(t) \\ & + (-\hat{A}_+\sin\phi_0\sin2\psi + \hat{A}_\times\cos\phi_0\cos2\psi)F^Y_\times(t)h^Y_s(t). \end{aligned} \tag{6}$$

This can be separated into a sum over four detector-independent amplitude parameters $\{\mathcal{A}^\mu\}$ and four detector-dependent polarization-weighted waveforms $\{h^Y_\mu(t)\}$,

$$s^Y(t) = \sum_{\mu=1}^{4} \mathcal{A}^\mu h^Y_\mu(t). \tag{7}$$

It is readily apparent that the amplitude parameters are defined as

$$\begin{aligned} \mathcal{A}^1 &:= \hat{A}_+\cos\phi_0\cos2\psi - \hat{A}_\times\sin\phi_0\sin2\psi, \\ \mathcal{A}^2 &:= \hat{A}_+\cos\phi_0\sin2\psi + \hat{A}_\times\sin\phi_0\cos2\psi, \\ \mathcal{A}^3 &:= -\hat{A}_+\sin\phi_0\cos2\psi - \hat{A}_\times\cos\phi_0\sin2\psi, \\ \mathcal{A}^4 &:= -\hat{A}_+\sin\phi_0\sin2\psi + \hat{A}_\times\cos\phi_0\cos2\psi, \end{aligned} \tag{8}$$

while the polarization-weighted waveforms are defined as

$$h_1^Y(t) := F_+^Y(t)h_c(t-t^Y), \qquad h_2^Y(t) := F_\times^Y(t)h_c(t-t^Y),$$
$$h_3^Y(t) := F_+^Y(t)h_s(t-t^Y), \qquad h_4^Y(t) := F_\times^Y(t)h_s(t-t^Y). \tag{9}$$

Turning our attention to the detector polarization responses, these characterize the response of an arbitrary GW detector for signals that satisfy the long-wavelength limit approximation [20]. They can be defined as the double contraction of two tensors [19],

$$F_+^Y(t) := \epsilon_+^{ij} d_{ij}^Y(t), \qquad F_\times^Y(t) := \epsilon_\times^{ij} d_{ij}^Y(t), \tag{10}$$

where $d_{ij}^Y(t)$ is the detector response tensor and $\{\epsilon_{+,\times}^{ij}\}$ are the polarization-independent basis tensors of the radiation frame. For an interferometric detector, the detector response tensor is given by

$$d_{ij}^Y(t) = \frac{1}{2}\{\hat{l}_1^Y(t)\otimes\hat{l}_1^Y(t) - \hat{l}_2^Y(t)\otimes\hat{l}_2^Y(t)\}_{ij}. \tag{11}$$

Here, $\hat{l}_1^Y$ is the unit vector pointing along interferometer Y's first arm away from the interferometer's vertex. Similarly, $\hat{l}_2^Y$ is the unit vector pointing along interferometer Y's second arm away from the interferometer's vertex. The polarization-independent basis tensors are defined as

$$\epsilon_+^{ij} := \{\hat{\xi}\otimes\hat{\xi} - \hat{\eta}\otimes\hat{\eta}\}^{ij}, \quad \epsilon_\times^{ij} := \{\hat{\xi}\otimes\hat{\eta} + \hat{\eta}\otimes\hat{\xi}\}^{ij}, \tag{12}$$

given in the radiation frame $\{\hat{\xi}, \hat{\eta}, -\hat{n}\}$, where $-\hat{n}$ is the direction of propagation, and $\{\hat{\xi}, \hat{\eta}\}$ are basis vectors in the wave plane (i.e., the plane perpendicular to the direction of propagation). The basis vectors $\hat{\xi}$ and $\hat{\eta}$ can be defined with respect to $\hat{n}$ as

$$\hat{\xi} := \frac{\hat{n}\times\hat{z}}{|\hat{n}\times\hat{z}|}, \qquad \hat{\eta} := \hat{\xi}\times\hat{n}. \tag{13}$$

In a fixed reference frame centered at the geocenter, where

$$\hat{n} = (\cos\delta\cos\alpha, \cos\delta\sin\alpha, \sin\delta), \tag{14}$$

the wave-plane basis vectors are

$$\hat{\xi} = (\sin\alpha, -\cos\alpha, 0), \tag{15}$$

$$\hat{\eta} = (-\sin\delta\cos\alpha, -\sin\delta\sin\alpha, \cos\delta). \tag{16}$$

We have now defined all of the quantities that are used to convert a GW signal from an arbitrary nonprecessing rotating quadrupole moment source to the signal seen by a GW detector. The remaining details of the signal will depend on the specifics of the emitting system.

III. THE $\mathcal{F}$-STATISTIC

The likelihood ratio of a signal $\boldsymbol{s}$ being in the data of a network of GW detectors $\boldsymbol{x}$ is given as

$$\Lambda(\boldsymbol{x};\boldsymbol{s}) = \frac{P(\boldsymbol{x}|\boldsymbol{s})}{P(\boldsymbol{x}|0)} = \exp\left[(\boldsymbol{x}|\boldsymbol{s}) - \frac{1}{2}(\boldsymbol{s}|\boldsymbol{s})\right], \tag{17}$$

where $(\boldsymbol{a}|\boldsymbol{b}) := \sum_Y (a^Y|b^Y)$ and the definition of the noise-weighted inner product $(a^Y|b^Y)$ depends on the details of the waveform being studied. We define this for inspiral signals in (26) of Sec. IV. Using the signal model from (7) and (17) can be written as

$$\ln\Lambda(\boldsymbol{x};\boldsymbol{s}) = \mathcal{A}^\mu x_\mu - \frac{1}{2}\mathcal{A}^\mu\mathcal{M}_{\mu\nu}\mathcal{A}^\nu, \tag{18}$$

where $x_\mu := (\boldsymbol{x}|\boldsymbol{h}_\mu)$ and $\mathcal{M}_{\mu\nu} := (\boldsymbol{h}_\mu|\boldsymbol{h}_\nu)$. In matrix form, $\mathcal{M}_{\mu\nu}$ is block diagonal,

$$\mathcal{M}_{\mu\nu} = \begin{pmatrix} A & C & 0 & 0 \\ C & B & 0 & 0 \\ 0 & 0 & A & C \\ 0 & 0 & C & B \end{pmatrix}_{\mu\nu}, \tag{19}$$

due to the orthogonality of the sine and cosine intrinsic waveforms. Here,

$$A := \sum_Y F_+^Y(t)F_+^Y(t)(h_c^Y|h_c^Y), \tag{20a}$$
$$B := \sum_Y F_\times^Y(t)F_\times^Y(t)(h_c^Y|h_c^Y), \tag{20b}$$
$$C := \sum_Y F_+^Y(t)F_\times^Y(t)(h_c^Y|h_c^Y). \tag{20c}$$

The log-likelihood ratio of (18) can be analytically maximized over the amplitude parameters, resulting in the maximum likelihood ratio $\mathcal{F}$-statistic [4],

$$\mathcal{F} := \ln\Lambda(\boldsymbol{x};\boldsymbol{s}_{\rm ML}) = \frac{1}{2}x_\mu\mathcal{M}^{\mu\nu}x_\nu, \tag{21}$$

where $\mathcal{M}^{\mu\nu} := \{\mathcal{M}^{-1}\}^{\mu\nu}$ is the inverse of $\mathcal{M}_{\mu\nu}$, i.e. $\mathcal{M}^{\mu\alpha}\mathcal{M}_{\alpha\nu} = \delta^\mu_\nu$, and takes the following form:

$$\mathcal{M}^{\mu\nu} = \frac{1}{D}\begin{pmatrix} B & -C & 0 & 0 \\ -C & A & 0 & 0 \\ 0 & 0 & B & -C \\ 0 & 0 & -C & A \end{pmatrix}^{\mu\nu}, \tag{22}$$

where $D := AB - C^2$. It should be noted that the $\mathcal{F}$-statistic is the same as the square of coherent SNR ($2\mathcal{F} = \rho_{\rm coh}^2$), which has been previously used in literature associated with coherent searches for inspiral signals with ground-based GW detectors [4,5].

IV. APPLICATION TO INSPIRAL SIGNALS

So far our treatment of the $\mathcal{F}$-statistic could be equally applied to searching for GW signals from rotating neutron stars or inspiraling binaries of compact objects. Restricting ourselves to the case of nonspinning inspiral signals, the intrinsic parameters include $\{\eta, \mathcal{M}_c\}$, where $\eta := m_1m_2/(m_1+m_2)^2$ is the symmetric mass ratio and

$\mathcal{M}_c := (m_1 + m_2)\eta^{3/5}$ is the chirp mass. In addition, there is an extrinsic parameter that can be efficiently maximized over but has not been in deriving the $\mathcal{F}$-statistic, namely the coalescence time t_c. This can be easily done with the use of the fast Fourier transform. The additional extrinsic parameters that must be searched over with separate filters are the sky locations $\{\alpha, \delta\}$, where α is the right ascension and δ is the declination.

Although we restrict the derivation to the case of short-duration nonspinning inspiral signals, spins aligned with the angular momentum could easily be incorporated into the phase model and included as intrinsic parameters. This is because binaries in which the objects' spins are aligned with the angular momentum do not precess.

In second-generation GW detectors, the sensitive band of the detectors will start as low as 10 Hz. A binary neutron star system's GW signal will be in the sensitive band of the detectors for $\lesssim 17$ minutes before coalescing, which amounts to a rotation of the Earth of $\lesssim 0.07$ radians. Thus, for a source's fixed sky location, the detectors can be approximated as fixed $d^Y_{ij}(t) \approx d^Y_{ij}(t_c)$. With this approximation, the polarization weighted waveforms are given in the frequency domain as

$$\begin{aligned} h^Y_1(f) &:= F^Y_+ h_c(f), \qquad & h^Y_2(f) &:= F^Y_\times h_c(f), \\ h^Y_3(f) &:= F^Y_+ h_s(f), \qquad & h^Y_4(f) &:= F^Y_\times h_s(f). \end{aligned} \tag{23}$$

The frequency domain intrinsic waveforms are given as

$$h_c(f) := \mathrm{A}(f)\Re e^{i\Psi(f)}, \qquad h_s(f) := \mathrm{A}(f)\Im e^{i\Psi(f)}, \tag{24}$$

where $\mathrm{A}(f)$ is the intrinsic amplitude of the waveform, $\Psi(f)$ is the phase of the waveform, and $\Re$ and $\Im$ denote operators that extract the real and imaginary parts, respectively. Each of these components has the following dependencies:

$$\begin{aligned} F^Y_+ &= F^Y_+(t_c; \alpha, \delta), \qquad & F^Y_\times &= F^Y_\times(t_c; \alpha, \delta), \\ \mathrm{A}(f) &= \mathrm{A}(f; \mathcal{M}_c, \eta), \qquad & \Psi(f) &= \Psi(f; t_c, \alpha, \delta, \mathcal{M}_c, \eta). \end{aligned} \tag{25}$$

Note that $\mathrm{A}(f)$ is typically defined to include h_0 and $\Psi(f)$ is typically defined (e.g., [9]) to include ϕ_0; however, in this treatment, h_0 and ϕ_0 are instead included as part of the amplitude parameters. The explicit expressions of $\mathrm{A}(f)$ and $\Psi(f)$ according to the stationary phase approximation are expanded to Newtonian order in the amplitude and 3.5 PN order in the phase in Appendix A.

The template waveforms for inspiral signals occupy a large bandwidth within the detectors, entering the sensitive band at the lower frequency cutoff f_{low} and extending up to the frequency associated with the innermost stable circular orbit f_{ISCO}. For these signals, the inner product between two waveforms is defined as

$$(x^Y|y^Y) := 4\Re \int_{f_{\mathrm{low}}}^{f_{\mathrm{high}}} \frac{\tilde{x}^Y(f)\tilde{y}^{Y*}(f)}{S^Y(f)} df, \tag{26}$$

where f_{high} is the upper cutoff frequency given by the smaller of the Nyquist frequency of the data and f_{ISCO}, $\tilde{x}(f)$ denotes the Fourier transform of $x(t)$, $(.)^*$ denotes the complex conjugate operator, and $S^Y(f)$ is the one-sided power spectral density (PSD) of detector Y.

V. $\mathcal{F}$-STATISTIC METRIC DERIVATION

The metric on the full set of parameters $\{\lambda\}$ including intrinsic and extrinsic parameters can be derived by expanding the log-likelihood ratio (17) for a mismatched signal to second order in the parameter differences, $\Delta\lambda$,

$$\begin{aligned} &2\ln\Lambda(\boldsymbol{s}(\lambda); \boldsymbol{s}(\lambda + \Delta\lambda)) \\ &\quad = (\boldsymbol{s}(\lambda)|\boldsymbol{s}(\lambda)) - (\partial_a \boldsymbol{s}(\lambda)|\partial_b \boldsymbol{s}(\lambda))\Delta\lambda^a\Delta\lambda^b + O(\Delta\lambda^3), \end{aligned} \tag{27}$$

where $\partial_a := \partial/\partial\lambda^a$ is the partial derivative w.r.t. parameter λ^a. In this notation, we will restrict the use of greek indices to the amplitude parameters (i.e., $\lambda^\mu = \mathcal{A}^\mu$) and for the metric subspace associated with the amplitude parameters. Using (27), we are led to the definition of the full metric g_{ab}, which measures the fractional loss of $2\mathcal{F}$, as

$$g_{ab} := \frac{(\partial_a \boldsymbol{s}|\partial_b \boldsymbol{s})}{(\boldsymbol{s}|\boldsymbol{s})}. \tag{28}$$

Recalling that $(\partial_\mu \mathcal{A}^\alpha \boldsymbol{h}_\alpha|\partial_\nu \mathcal{A}^\beta \boldsymbol{h}_\beta) = (\boldsymbol{h}_\mu|\boldsymbol{h}_\nu) = \mathcal{M}_{\mu\nu}$, and using the signal model from (7), this metric can be decomposed into blocks

$$g_{ab} = \frac{1}{\mathcal{A}^\alpha \mathcal{M}_{\alpha\beta} \mathcal{A}^\beta} \begin{pmatrix} \mathcal{M}_{\mu\nu} & \mathcal{A}^\alpha \mathcal{R}_{\mu\alpha j} \\ \mathcal{A}^\beta \mathcal{R}_{\nu\beta i} & \mathcal{A}^\alpha h_{\alpha\beta ij} \mathcal{A}^\beta \end{pmatrix}_{ab}. \tag{29}$$

As stated before, in the above equation, the indices μ and ν are associated with the amplitude parameter subspace and the indices i and j are associated with the nonamplitude parameter subspace. The quantities $\mathcal{R}_{\mu\nu i}$ and $h_{\mu\nu ij}$ are defined as

$$\mathcal{R}_{\mu\nu i} := (\boldsymbol{h}_\mu|\partial_i \boldsymbol{h}_\nu), \tag{30}$$

$$h_{\mu\nu ij} := (\partial_i \boldsymbol{h}_\mu|\partial_j \boldsymbol{h}_\nu). \tag{31}$$

The $\mathcal{M}_{\mu\nu}$ block is associated with derivatives of only the amplitude parameter subspace, the $\mathcal{A}^\alpha h_{\alpha\beta ij} \mathcal{A}^\beta$ block only with derivatives of the nonamplitude parameter subspace, and the $\mathcal{A}^\alpha \mathcal{R}_{\mu\alpha i}$ block with derivatives of both subspaces.

To obtain the metric for the $\mathcal{F}$-statistic, we can project out the dimensions associated with the amplitude subspace [13,21]

$$g^{\mathcal{F}}_{ij} = g_{ij} - g_{i\alpha} g^{\alpha\beta} g_{\beta j}. \tag{32}$$

Using the form of the full metric from (29), the $\mathcal{F}$-statistic metric can be written as

$$g^{\mathcal{F}}_{ij} = \frac{\mathcal{A}^\alpha \mathcal{G}_{\alpha\beta ij} \mathcal{A}^\beta}{\mathcal{A}^\alpha \mathcal{M}_{\alpha\beta} \mathcal{A}^\beta}, \tag{33}$$

where the projected Fisher matrix $\mathcal{G}_{\mu\nu ij}$ is given by

$$\mathcal{G}_{\mu\nu ij} = h_{\mu\nu ij} - \mathcal{R}_{\alpha\mu i}\mathcal{M}^{\alpha\beta}\mathcal{R}_{\beta\nu j}. \tag{34}$$

The two pieces of the projected Fisher matrix we refer to as he nonamplitude parameter subspace matrix, $h_{\mu\nu ij}$, and the amplitude subspace maximization correction, $\mathcal{R}_{\alpha\mu i}\mathcal{M}^{\alpha\beta}\mathcal{R}_{\beta\nu j}$. Similar to the derivation in Appendix B of Ref. [13], after symmetrizing on (μ, ν) and (i, j), $h_{\mu\nu ij}$ takes the form

$$h_{\mu\nu ij} = \begin{pmatrix} P^1_{ij} & P^3_{ij} & 0 & P^4_{ij} \\ P^3_{ij} & P^2_{ij} & -P^4_{ij} & 0 \\ 0 & -P^4_{ij} & P^1_{ij} & P^3_{ij} \\ P^4_{ij} & 0 & P^3_{ij} & P^2_{ij} \end{pmatrix}_{\mu\nu}. \tag{35}$$

Although this looks identical to the derivation for rotating neutron star signals [13], one difference to keep in mind is that for inspiral signals there are additional terms hidden in these components. These additional terms are the result of the presence of an intrinsic parameter in the amplitude of the signal, what we refer to as the intrinsic amplitude. This can be seen in (25). The components of $h_{\mu\nu ij}$ are given as

$$P^1_{ij} = \boldsymbol{f}^{++}\cdot\boldsymbol{G}_{ij} + \boldsymbol{f}^{++}_i\cdot\boldsymbol{J}_j + \boldsymbol{f}^{++}_j\cdot\boldsymbol{J}_i + \boldsymbol{f}^{++}_{ij}\cdot\boldsymbol{H}, \tag{36a}$$

$$P^2_{ij} = \mathbf{f}^{\times\times}\cdot\mathbf{G}_{ij} + \mathbf{f}^{\times\times}_i\cdot\mathbf{J}_j + \mathbf{f}^{\times\times}_j\cdot\mathbf{J}_i + \mathbf{f}^{\times\times}_{ij}\cdot\mathbf{H}, \tag{36b}$$

$$P^3_{ij} = \boldsymbol{f}^{+\times}\cdot\boldsymbol{G}_{ij} + \frac{1}{2}(\boldsymbol{f}^{+\times}_i + \boldsymbol{f}^{\times+}_i)\cdot\boldsymbol{J}_j + \frac{1}{2}(\boldsymbol{f}^{+\times}_j + \boldsymbol{f}^{\times+}_j)\cdot\boldsymbol{J}_i + \frac{1}{2}(\boldsymbol{f}^{+\times}_{ij} + \boldsymbol{f}^{\times+}_{ij})\cdot\boldsymbol{H}, \tag{36c}$$

$$P^4_{ij} = \frac{1}{2}(\boldsymbol{f}^{+\times}_i - \boldsymbol{f}^{\times+}_i)\cdot\boldsymbol{K}_j + \frac{1}{2}(\boldsymbol{f}^{+\times}_j - \boldsymbol{f}^{\times+}_j)\cdot\boldsymbol{K}_i. \tag{36d}$$

Above, we have introduced the detectors' polarization response vectors $\boldsymbol{f}^{pq}_{(ij)}$, the detectors' waveform vectors $\{\boldsymbol{H}, \boldsymbol{J}_i, \boldsymbol{K}_i, \boldsymbol{G}_{ij}\}$, and the notation $\boldsymbol{x}\cdot\boldsymbol{y} := \sum_Y x^Y y^Y$, which denotes a sum over detectors. The detectors' polarization response vectors are defined as

$$f^{pqY} := F^Y_p F^Y_q, \tag{37}$$

$$f^{pqY}_i := \partial_i F^Y_p F^Y_q, \tag{38}$$

$$f^{pqY}_{ij} := \partial_i F^Y_p \partial_j F^Y_q, \tag{39}$$

where the derivatives of the detector polarization responses $\partial_i F^Y_{+,\times}$ are given in Appendix B. Next, the detectors' waveform vectors $\{\boldsymbol{H}, \boldsymbol{J}_i, \boldsymbol{K}_i, \boldsymbol{G}_{ij}\}$ are defined as

$$G^Y_{ij} := (h^Y\partial_i \ln\mathrm{A}|h^Y\partial_j \ln\mathrm{A}) + (h^Y\partial_i\Psi^Y(f)|h^Y\partial_j\Psi^Y(f)), \tag{40}$$

$$H^Y := (h^Y|h^Y), \tag{41}$$

$$J^Y_i := (h^Y|h^Y\partial_i \ln\mathrm{A}), \tag{42}$$

$$K^Y_i := (h^Y|h^Y\partial_i\Psi(f)), \tag{43}$$

where the terms $(h^Y|h^Y)$, $(h^Y|h^Y\partial_i \ln\mathrm{A})$, $(h^Y|h^Y\partial_i\Psi^Y(f))$, $(h^Y\partial_i \ln\mathrm{A}|h^Y\partial_j \ln\mathrm{A})$, and $(h^Y\partial_i\Psi^Y(f)|h^Y\partial_j\Psi^Y(f))$ are given in Appendix C. As referred to above, the additional terms for inspiral signals associated with derivatives of the intrinsic amplitude are contained in the $\boldsymbol{G}_{ij}$ and $\boldsymbol{J}_i$ terms.

Looking at the amplitude subspace maximization correction, $\mathcal{R}_{\alpha\mu i}\mathcal{M}^{\alpha\beta}\mathcal{R}_{\beta\nu j}$, $\mathcal{R}_{\mu\nu i}$ has the block form

$$\mathcal{R}_{\mu\nu i} = \begin{pmatrix} \hat{\mathcal{R}}_i & \tilde{\mathcal{R}}_i \\ -\tilde{\mathcal{R}}_i & \hat{\mathcal{R}}_i \end{pmatrix}_{\mu\nu}, \tag{44}$$

where the blocks $\hat{\mathcal{R}}_i$ and $\tilde{\mathcal{R}}_i$ are defined as

$$\hat{\mathcal{R}}_i := \begin{pmatrix} R^{11}_i & R^{12}_i \\ R^{21}_i & R^{22}_i \end{pmatrix}, \quad \text{and} \quad \tilde{\mathcal{R}}_i := \begin{pmatrix} R^{13}_i & R^{14}_i \\ R^{14}_i & R^{24}_i \end{pmatrix}. \tag{45}$$

These components are defined in Appendix D. As noted in Appendix B of Ref. [13], $\tilde{\mathcal{R}}_i$ contains only terms with derivatives of the phase. However for the case of inspiral signals, $\hat{\mathcal{R}}_i$ also contains terms with derivatives of both the antenna factors and the intrinsic amplitude. After using the symmetries of (22) and (44), and symmetrizing on (i, j), the final form for $\mathcal{R}_{\alpha\mu i}\mathcal{M}^{\alpha\beta}\mathcal{R}_{\beta\nu j}$ is

$$\mathcal{R}_{\alpha\mu i}\mathcal{M}^{\alpha\beta}\mathcal{R}_{\beta\nu j} = \begin{pmatrix} Q^1_{ij} & Q^3_{ij} & 0 & Q^4_{ij} \\ Q^3_{ij} & Q^2_{ij} & -Q^4_{ij} & 0 \\ 0 & -Q^4_{ij} & Q^1_{ij} & Q^3_{ij} \\ Q^4_{ij} & 0 & Q^3_{ij} & Q^2_{ij} \end{pmatrix}_{\mu\nu}. \tag{46}$$

Explicit expressions for the Q components are given in Appendix D.

Combining the terms from (35) and (46), we find the projected Fisher matrix for inspiral signals has the same form as that of the low-frequency limit of rotating neutron star signals (i.e., Appendix B of Ref. [13]),

$$\mathcal{G}_{\mu\nu ij} = \begin{pmatrix} m^1_{ij} & m^3_{ij} & 0 & m^4_{ij} \\ m^3_{ij} & m^2_{ij} & -m^4_{ij} & 0 \\ 0 & -m^4_{ij} & m^1_{ij} & m^3_{ij} \\ m^4_{ij} & 0 & m^3_{ij} & m^2_{ij} \end{pmatrix}_{\mu\nu}, \tag{47}$$

where $m^k_{ij} = P^k_{ij} - Q^k_{ij}$. Combining (33) and (47) gives the main result of this paper, namely, the coherent $\mathcal{F}$-statistic metric for short-duration nonprecessing inspiral signals.

It should be noted that, as in the rotating neutron star case, although the $\mathcal{F}$-statistic metric (33) has projected out the amplitude parameter subspace, it is still dependent on the amplitude parameters. This means that what has been

derived is actually a family of metrics that depend on the extrinsic parameters that enter the amplitude parameters [13]. In order to produce a metric that is useful for choosing template points to cover the parameter space, we must choose an averaging procedure. As an example, Prix takes the average of the eigenvalues of $(\mathcal{M}^{\alpha\beta}\mathcal{G}_{\alpha\beta ij}\Delta\lambda^i\Delta\lambda^j)$ to produce an average metric. This is motivated by the fact that this matrix determines the extremal mismatches that can be obtained for any combination of amplitude parameters [13,22].

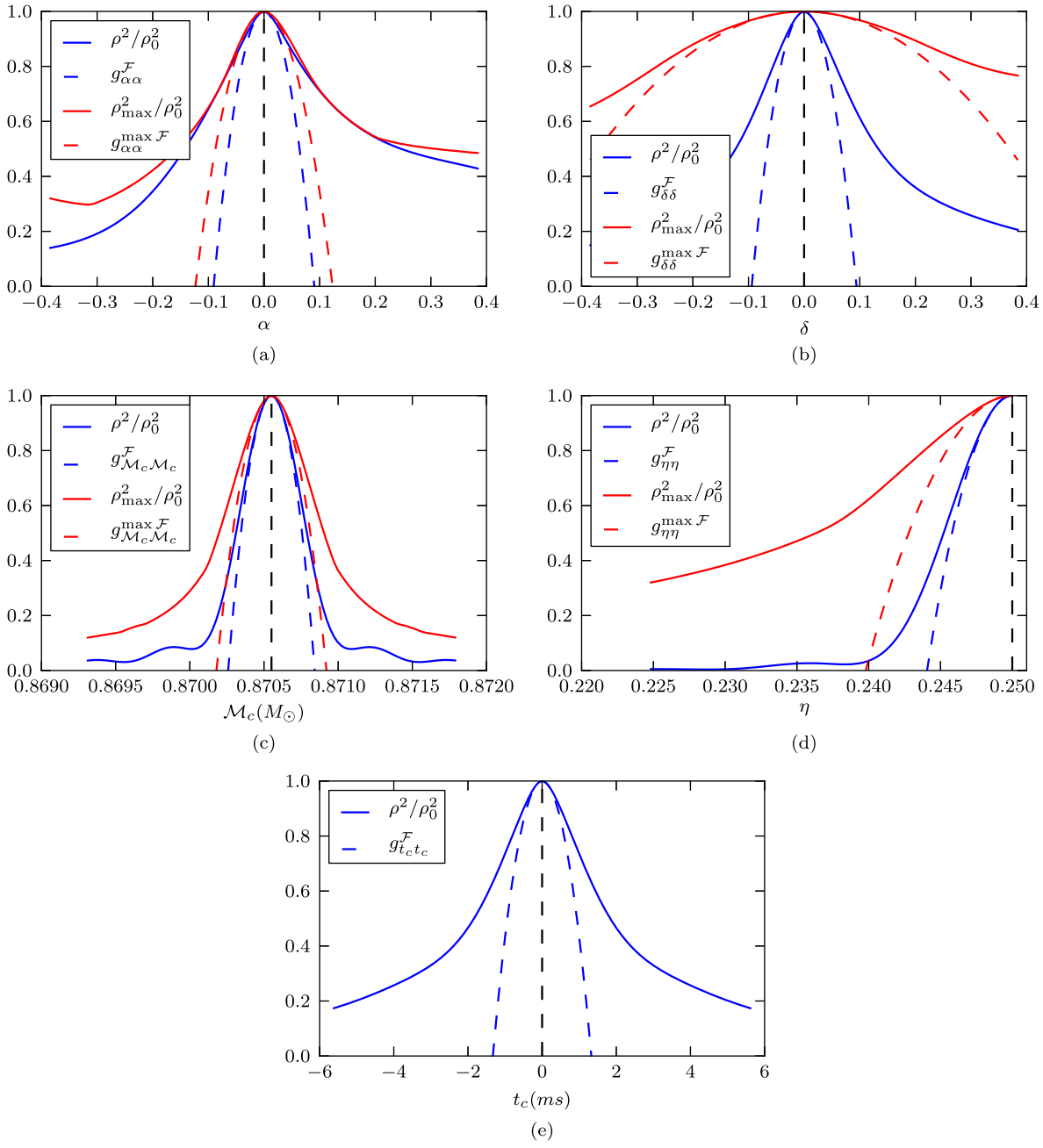

FIG. 1 (color online). We show the fractional loss of $\mathcal{F}$ as a function of parameter mismatches for the coherent analysis, using the Advanced LIGO and Advanced Virgo detectors, of an inspiral signal with component masses $m_1 = m_2 = 1.4M_\odot$, sky location $(\alpha, \delta) = (0, 0)$, coalescence time $t_c = 0$, reference phase $\phi_0 = 0$, polarization phase $\psi = 0$, cosine of the inclination angle $\cos\iota = 1$, and distance $\mathcal{D} = 200$ Mpc. The vertical line shows the true parameters of the injected signal. The solid lines show the observed fractional $\mathcal{F}$ with and without maximization over time (where appropriate). The dashed lines show the predicted fractional $\mathcal{F}$ from the coherent metric, without $(g^{\mathcal{F}}_{\mu\mu})$ and with $(g^{\max\mathcal{F}}_{\mu\mu})$ projection of the time dimension of the metric. The metric accurately predicts the fractional loss of $\mathcal{F}$ above a match of ~0.95. Panels (a), (b), (c), (d), and (e) show the mismatch associated variations of the right ascension, declination, chirp mass, symmetric mass ratio, and coalescence time, respectively.

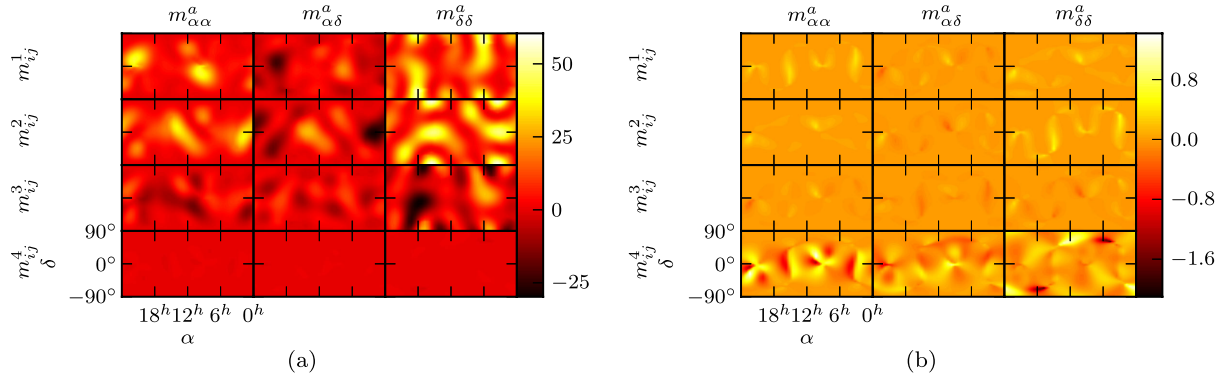

FIG. 2 (color online). We show the separate mismatch components of the metric, m^k_{ij} of (47), as functions of sky position in (a). The parts of m^k_{ij} associated with the derivatives of the detector response are shown in (b). For the first three mismatches, these terms are typically more than an order of magnitude smaller than the full mismatches.

VI. VERIFICATION

With the $\mathcal{F}$-statistic metric for short-duration nonprecessing inspiral signals in hand, we can verify its performance by comparing the fractional loss of the $\mathcal{F}$-statistic for mismatched signals to that predicted by the metric. We do this using a network of detectors corresponding to the locations and orientations of the LIGO Hanford, LIGO Livingston, and Virgo detectors. The PSD we use for the LIGO detectors is the zero-detuning high-power advanced detector configuration [23]. For Virgo, we use the advanced detector PSD [24]. The waveform model used for this work is the nonspinning restricted TaylorF2 PN approximation [25,26], which is given in Appendix A. For computational reasons, we start the waveforms at a low-frequency cutoff of 40 Hz, although our results should also be valid for other choices of the low-frequency cutoff.

We perform our tests using the following intrinsic parameters for the injected signal: $m_1 = m_2 = 1.4M_\odot$. The extrinsic parameters are $(\alpha, \delta) = (0, 0)$, $t_c = 0$, $\phi_0 = 0$, $\psi = 0, \cos\iota = 1$, and $\mathcal{D} = 200$ Mpc. The expected square coherent SNR for this signal is $2\mathcal{F} = 9.8^2$. We check the metric by computing the match, both with and without maximization over time, while varying a single parameter. We do this for the two intrinsic parameters $\{\mathcal{M}_c, \eta\}$, for the two extrinsic sky-location parameters $\{\alpha, \delta\}$, and also for the time parameter $\{t_c\}$. Figure 1(a) shows how the match varies when the template's right ascension deviates from the signal's value, shown as the vertical line. The metric reliably predicts the observed loss in $\mathcal{F}$ above $\sim$0.95.

We are interested to see the effect that including derivatives of the detector responses has on the metric calculation. To do this, first we check the mismatches m^a_{ij} from (47) associated with the $\mathcal{F}$-statistic metric as a function of sky location, which can be seen in Fig. 2(a). Figure 2(b) shows the portion of these mismatches that originates from the derivatives of the detector responses. We see that for the first three mismatches, this portion is typically an order of magnitude smaller than the full mismatch. As the fourth mismatch is already an order of magnitude smaller than the first three, including these terms is generally only a small correction to the metric. However, as we shall see, there are points in parameter space where this is not true.

Finally, we check the effect of including the derivatives of the detector responses in the metric in an extreme example. We use the following intrinsic parameters for the injected signal: $m_1 = m_2 = 1.4M_\odot$. The extrinsic parameters are $(\alpha, \delta) = (0.785, -0.785)$, $t_c = 0$, $\phi_0 = 0$, $\psi = 0$, $\cos\iota = 1$, $\mathcal{D} = 9.3$ Mpc. The distance is an order of magnitude smaller than the previous comparisons in order to obtain an equal expected square coherent SNR for this signal, $2\mathcal{F} = 9.8^2$. Figure 3 compares the predictions from the metric derived with and without the derivatives of detector responses to the observed time-maximized fractional loss of $\mathcal{F}$. We see that the predictions from the metric that includes the derivatives of the detector responses give a substantially better match to the observed time-maximized fractional loss

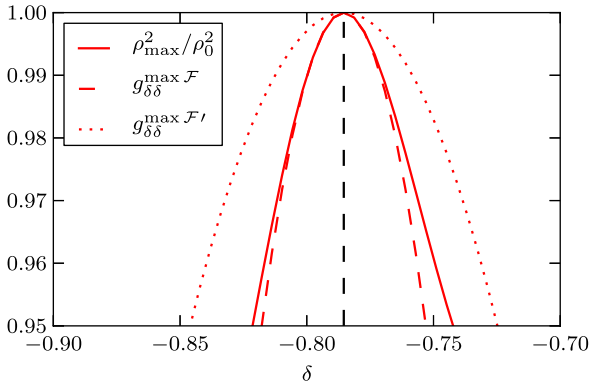

FIG. 3 (color online). We compare the time-maximized $\mathcal{F}$-statistic metric component with and without the derivatives of the detector responses, denoted as $g^{\max\mathcal{F}}_{\delta\delta}$ and $g^{\max\mathcal{F}\prime}_{\delta\delta}$, respectively, for a specific set of parameter space coordinates: component masses $m_1 = m_2 = 1.4M_\odot$, sky location $(\alpha, \delta) = (0.785, -0.785)$, coalescence time $t_c = 0$, reference phase $\phi_0 = 0$, polarization phase $\psi = 0$, cosine of the inclination angle $\cos\iota = 1$, and distance $\mathcal{D} = 9.3$ Mpc. The metric derived with the derivatives of detector responses better matches the observed time-maximized fractional loss of $\mathcal{F}$.

of $\mathcal{F}$. However, it should be noted that the detector network is much less sensitive to this point, which was chosen especially to show a large discrepancy between including versus not including those derivatives. For the majority of parameter space, the discrepancy is much smaller.

VII. CONCLUSION

In this work, we derive the coherent $\mathcal{F}$-statistic metric associated with short-duration nonprecessing inspiral signals. This metric, understandably, has very close ties to the coherent $\mathcal{F}$-statistic metric associated with rotating neutron star signals. However, in detail, there are several important differences. For one, inspiral signals have a larger bandwidth; hence, the important single-detector quantities are not the detectors' PSD values at a single frequency, but the integrated noise moments of the detectors' PSDs. Second, the signal model includes intrinsic parameters in the amplitude, which need to be properly accounted for in the metric derivation.

Even though this derivation closely follows that for the rotating neutron star case, it includes previously ignored effects of the variation of the detector responses. If desired, this could easily be incorporated into the rotating neutron star coherent $\mathcal{F}$-statistic metric for a more complete picture of the sky-tiling problem.

Important aspects that should be explored in the future include determining other ways that the amplitude-dependent metric, derived here, can be averaged [13] and applying the averaged metric to the template covering problem associated with coherent searches for short-duration nonprecessing inspiral signals. In order to efficiently perform this search, it will need to be investigated how well the metric can be separated into an intrinsic parameter space (e.g., the mass space) and an extrinsic parameter space (e.g., the sky space) that could be tiled separately. This would allow filters associated with different intrinsic parameters to be reused for the extrinsic parameters that still need to be searched in a tiled manner [11,18].

Finally, because of the close ties between the metric and the projected Fisher matrix, it may be interesting to use the derivation here to determine the sky localization accuracy of a detector network, which could then be compared to the derivations of [14,15,27–29].

ACKNOWLEDGMENTS

The author would like to acknowledge many useful discussions with Sukanta Bose, Badri Krishnan, and Reinhard Prix that this work is based upon. The author would also like to thank Thomas Dent, Alex Nielsen, and Chris Pankow for useful comments on this manuscript. The author is supported by the Max Planck Gesellschaft. Numerical overlap calculations in this work were accelerated using PYCUDA [30]. This document has LIGO Document No. LIGO-P1200091.

APPENDIX A: TAYLORF2 PN WAVEFORM

In this section we give the explicit formulas for the restricted SPA TaylorF2 inspiral waveform. As noted in Sec. IV, the inspiral waveform can be split into three pieces, a frequency-independent extrinsic amplitude (i.e., a function of only extrinsic parameters), a frequency-dependent intrinsic amplitude (i.e., a function of intrinsic parameters and frequency), and a phase piece that depends on intrinsic parameters, extrinsic parameters, and frequency. The extrinsic amplitude for a signal at distance $\mathcal{D}$ is given by

$$h_0 = \sqrt{\frac{5}{24}}\frac{1}{\pi^{2/3}\mathcal{D}}, \tag{A1}$$

and the intrinsic amplitude for a signal with chirp mass $\mathcal{M}_c$ is

$$\mathrm{A}(f) = \mathcal{M}_c^{-5/3} f^{-7/6}. \tag{A2}$$

For convenience, we define A without the frequency dependence as

$$\mathrm{A} := \mathcal{M}_c^{-5/3}. \tag{A3}$$

The phase of the inspiral waveform, expanded to 3.5 PN order, can be written as

$$\Psi^Y(f) = 2\pi f t^Y - \frac{\pi}{4} + \phi_0 + \sum_{j=0}^{7} \psi_j f^{(-5+j)/3} + \sum_{j=5}^{6} \psi_j^l \ln(f) f^{(-5+j)/3}, \tag{A4}$$

where $t^Y := t_c - \vec{r}_Y \cdot \hat{n}/c$ is a time parameter that includes the time of arrival of the end of the waveform at the geocenter t_c and the sky-location-dependent correction associated with a detector Y's location, and ψ_j and ψ_j^l are the phase coefficients associated with the $j/2$ PN order. These phase coefficients are given by

$$\psi_0 = \frac{3}{128\pi^{5/3}\mathcal{M}_c^{5/3}}, \tag{A5a}$$

$$\psi_2 = \frac{5}{384\pi\mathcal{M}_c\eta^{2/5}}\left(\frac{743}{84} + 11\eta\right), \tag{A5b}$$

$$\psi_3 = \frac{-3\pi^{1/3}}{8\mathcal{M}_c^{2/3}\eta^{3/5}}, \tag{A5c}$$

$$\psi_4 = \frac{5}{3072\pi^{1/3}\mathcal{M}_c^{1/3}\eta^{4/5}} \times \left(\frac{3058673}{7056} + \frac{5429}{7}\eta + 617\eta^2\right), \tag{A5d}$$

$$\psi_5 = \frac{5\pi}{384\eta}\left(\frac{7729}{84} - 13\eta\right) \times [1 + \log(6^{3/2}\pi\mathcal{M}_c\eta^{-3/5})], \tag{A5e}$$

$$\psi_5^l = \frac{5\pi}{384\eta}\left(\frac{7729}{84} - 13\eta\right), \tag{A5f}$$

$$\psi_6 = \frac{\pi^{1/3}\mathcal{M}_c^{1/3}}{128\eta^{6/5}}\left(\frac{11583231236531}{1564738560} - 640\pi^2 - \frac{6848}{7}[\gamma + \log(4\pi^{1/3}\mathcal{M}_c^{1/3}\eta^{-1/5})] + \frac{5}{4}\left[\frac{-3147553127}{254016} + 451\pi^2\right]\eta + \frac{76055}{576}\eta^2 - \frac{127825}{432}\eta^3\right), \tag{A5g}$$

$$\psi_6^l = \frac{-107\pi^{1/3}\mathcal{M}_c^{1/3}}{42\eta^{6/5}}, \tag{A5h}$$

$$\psi_7 = \frac{5\pi^{5/3}\mathcal{M}_c^{2/3}}{32256\eta^{7/5}} \times \left(\frac{15419335}{336} + \frac{75703}{2}\eta - 14809\eta^2\right). \tag{A5i}$$

Any PN coefficients of 3.5 PN order or lower not defined above are identically zero.

APPENDIX B: EXPLICIT EXPRESSIONS FOR DETECTOR POLARIZATION RESPONSE DERIVATIVES

Based on the expressions for the detector polarization responses in Sec. II and [19], the derivatives of the detector polarization responses can be obtained in terms of derivatives of the polarization-independent basis tensors,

$$\partial_a F^Y_{+,\times} = \partial_a \boldsymbol{\epsilon}^{ij}_{+,\times} d^Y_{ij}. \tag{B1}$$

These in turn can be written in terms of derivatives of the radiation frame basis vector,

$$\partial_a \boldsymbol{\epsilon}^{ij}_{+} = \{(\partial_a \vec{\xi}) \otimes \vec{\xi} + \vec{\xi} \otimes (\partial_a \vec{\xi}) - (\partial_a \vec{\eta}) \otimes \vec{\eta} - \vec{\eta} \otimes (\partial_a \vec{\eta})\}^{ij}, \tag{B2a}$$

$$\partial_a \boldsymbol{\epsilon}^{ij}_{\times} = \{(\partial_a \vec{\xi}) \otimes \vec{\eta} + \vec{\xi} \otimes (\partial_a \vec{\eta}) + (\partial_a \vec{\eta}) \otimes \vec{\xi} + \vec{\eta} \otimes (\partial_a \vec{\xi})\}^{ij}. \tag{B2b}$$

The explicit formulas for the derivatives of the radiation frame basis vectors with respect to the right ascension and declination are given as

$$\partial_\alpha \hat{n} = (-\cos\delta\sin\alpha, \cos\delta\cos\alpha, 0), \tag{B3a}$$

$$\partial_\delta \hat{n} = (-\sin\delta\cos\alpha, -\sin\delta\sin\alpha, \cos\delta), \tag{B3b}$$

$$\partial_\alpha \hat{\xi} = (\cos\alpha, \sin\alpha, 0), \tag{B3c}$$

$$\partial_\delta \hat{\xi} = (0, 0, 0), \tag{B3d}$$

$$\partial_\alpha \hat{\eta} = (\sin\delta\sin\alpha, -\sin\delta\cos\alpha, 0), \tag{B3e}$$

$$\partial_\delta \hat{\eta} = (-\cos\delta\cos\alpha, -\cos\delta\sin\alpha, -\sin\delta). \tag{B3f}$$

APPENDIX C: EXPLICIT EXPRESSIONS FOR INNER PRODUCT DERIVATIVES

In this section we define the inner products that are needed for the coherent $\mathcal{F}$-statistic for short-duration nonprecessing inspiral signals in terms of derivatives of intrinsic and extrinsic parameters and combinations of detector noise moment integrals, given by (E1) of Appendix E.

The simplest inner product required, which contains no derivatives, is used by $\mathcal{M}_{\mu\nu}$ and $\boldsymbol{H}$,

$$(h^Y|h^Y) = \mathrm{A}^2 I(7,0)^Y := H^Y. \tag{C1}$$

The inner product that contains a single derivative of the intrinsic amplitude and is used by $\boldsymbol{J}_i$ is

$$(h^Y|h^Y\partial_i \ln\mathrm{A}) = -\frac{5}{3}\frac{\partial \ln\mathcal{M}_c}{\partial\lambda^i}\mathrm{A}^2 I(7,0)^Y =: J^Y_i. \tag{C2}$$

The inner product that contains a single derivative of the phase and is used by $\boldsymbol{K}_i$ is

$$(h^Y|h^Y\partial_i\Psi^Y(f)) = \mathrm{A}^2\left(\frac{\partial t^Y}{\partial\lambda^i}2\pi I(4,0)^Y + \sum_k\left[\frac{\partial\psi_k}{\partial\lambda^i}I(12-k,0)^Y + \frac{\partial\psi^l_k}{\partial\lambda^i}I(12-k,1)^Y\right]\right) =: K^Y_i. \tag{C3}$$

Finally, the inner product that contains both two single derivatives of the intrinsic amplitude and two single derivatives of the phase is used by $\boldsymbol{G}_{ij}$,

$$(h^Y\partial_i\ln\mathrm{A}|h^Y\partial_j\ln\mathrm{A}) + (h^Y\partial_i\Psi^Y(f)|h^Y\partial_j\Psi^Y(f)) =: \boldsymbol{G}_{ij}. \tag{C4}$$

These individual inner products are given by

$$(h^Y\partial_i\ln\mathrm{A}|h^Y\partial_j\ln\mathrm{A}) = \frac{25}{9}\frac{\partial\ln\mathcal{M}_c}{\partial\lambda^i}\frac{\partial\ln\mathcal{M}_c}{\partial\lambda^j}\mathrm{A}^2 I(7,0)^Y, \tag{C5}$$

and

$$(h^Y\partial_i\Psi^Y(f)|h^Y\partial_j\Psi^Y(f)) = \mathrm{A}^2\Bigg[\frac{\partial t^Y}{\partial\lambda^i}\frac{\partial t^Y}{\partial\lambda^j}4\pi^2 I(1,0)^Y + \sum_k\Big(\frac{\partial t^Y}{\partial\lambda^i}\frac{\partial\psi_k}{\partial\lambda^j}+\frac{\partial\psi_k}{\partial\lambda^i}\frac{\partial t^Y}{\partial\lambda^j}\Big)2\pi I(9-k,0)^Y$$
$$+\sum_k\Big(\frac{\partial t^Y}{\partial\lambda^i}\frac{\partial\psi^l_k}{\partial\lambda^j}+\frac{\partial\psi^l_k}{\partial\lambda^i}\frac{\partial t^Y}{\partial\lambda^j}\Big)2\pi I(9-k,1)^Y + \sum_{k,l}\frac{\partial\psi_k}{\partial\lambda^i}\frac{\partial\psi_l}{\partial\lambda^j}I(17-k-l,0)^Y$$
$$+\sum_{k,l}\Big(\frac{\partial\psi_k}{\partial\lambda^i}\frac{\partial\psi^l_l}{\partial\lambda^j}+\frac{\partial\psi^l_k}{\partial\lambda^i}\frac{\partial\psi_l}{\partial\lambda^j}\Big)I(17-k-l,1)^Y + \sum_{k,l}\frac{\partial\psi^l_k}{\partial\lambda^i}\frac{\partial\psi^l_l}{\partial\lambda^j}I(17-k-l,2)^Y\Bigg]. \quad \text{(C6)}$$

APPENDIX D: EXPLICIT TERMS ASSOCIATED WITH $\mathcal{G}_{\mu\nu ij}$

The explicit formulas of the amplitude subspace maximization correction Q of the projected Fisher matrix, written in terms of the $R^{\mu\nu}_i$ components, are given as

$$DQ^1_{ij} = A(R^{21}_iR^{21}_j + R^{14}_iR^{14}_j) + B(R^{11}_iR^{11}_j + R^{13}_iR^{13}_j) - C(R^{11}_iR^{21}_j + R^{21}_iR^{11}_j + R^{13}_iR^{14}_j + R^{14}_iR^{13}_j), \quad \text{(D1a)}$$
$$DQ^2_{ij} = A(R^{22}_iR^{22}_j + R^{24}_iR^{24}_j) + B(R^{12}_iR^{12}_j + R^{14}_iR^{14}_j) - C(R^{12}_iR^{22}_j + R^{22}_iR^{12}_j + R^{14}_iR^{24}_j + R^{24}_iR^{14}_j), \quad \text{(D1b)}$$
$$DQ^3_{ij} = A(R^{21}_iR^{22}_j + R^{22}_iR^{21}_j + R^{14}_iR^{24}_j + R^{24}_iR^{14}_j) + B(R^{11}_iR^{12}_j + R^{12}_iR^{11}_j + R^{13}_iR^{14}_j + R^{14}_iR^{13}_j)$$
$$- C(R^{11}_iR^{22}_j + R^{22}_iR^{11}_j + R^{12}_iR^{21}_j + R^{21}_iR^{12}_j + R^{13}_iR^{24}_j + R^{24}_iR^{13}_j + 2R^{14}_iR^{14}_j), \quad \text{(D1c)}$$
$$DQ^4_{ij} = A(R^{21}_iR^{24}_j + R^{24}_iR^{21}_j - R^{14}_iR^{22}_j - R^{22}_iR^{14}_j) + B(R^{11}_iR^{14}_j + R^{14}_iR^{11}_j - R^{13}_iR^{12}_j - R^{12}_iR^{13}_j)$$
$$- C(R^{11}_iR^{24}_j + R^{24}_iR^{11}_j + R^{14}_iR^{21}_j + R^{21}_iR^{14}_j - R^{13}_iR^{22}_j - R^{22}_iR^{13}_j - R^{12}_iR^{14}_j - R^{14}_iR^{12}_j), \quad \text{(D1d)}$$

where we recall that A, B, C, D come from (22) for $\mathcal{M}^{\mu\nu}$. These R^{ij}_k components are given by

$$R^{11}_i = \boldsymbol{f}^{++}_i\cdot\boldsymbol{H} + \boldsymbol{f}^{++}\cdot\boldsymbol{J}_i, \quad \text{(D2a)}$$
$$R^{12}_i = \boldsymbol{f}^{\times+}_i\cdot\boldsymbol{H} + \boldsymbol{f}^{\times+}\cdot\boldsymbol{J}_i, \quad \text{(D2b)}$$
$$R^{21}_i = \boldsymbol{f}^{+\times}_i\cdot\boldsymbol{H} + \boldsymbol{f}^{+\times}\cdot\boldsymbol{J}_i, \quad \text{(D2c)}$$
$$R^{22}_i = \boldsymbol{f}^{\times\times}_i\cdot\boldsymbol{H} + \boldsymbol{f}^{\times\times}\cdot\boldsymbol{J}_i, \quad \text{(D2d)}$$
$$R^{13}_i = \boldsymbol{f}^{++}\cdot\boldsymbol{K}_i, \quad \text{(D2e)}$$
$$R^{14}_i = \boldsymbol{f}^{+\times}\cdot\boldsymbol{K}_i, \quad \text{(D2f)}$$
$$R^{24}_i = \boldsymbol{f}^{\times\times}\cdot\boldsymbol{K}_i. \quad \text{(D2g)}$$

It is interesting to note that all of the Q components contain terms associated with derivatives of the detector polarization responses as well as terms associated with derivatives of the intrinsic amplitude.

APPENDIX E: DETECTOR PSD MOMENT INTEGRALS

In this section we define the noise moment integrals $I(k,l)^Y$ of detector Y's PSD,

$$I(k,l)^Y := \frac{1}{\mathrm{A}^2}(h^Y|h^Y\ln^l(f)f^{-k/3}) = \int_{f_{\mathrm{low}}}^{f_{\mathrm{high}}}\frac{\ln^l(f)f^{-k/3}}{S^Y(f)}df. \quad \text{(E1)}$$

This is the same definition as in [9]. Based on the definition in (E1), it is easy to see that powers of the frequency in the inner product can be manipulated as $(h^Y\ln^{l_1}(f)f^{-k_1/3}|h^Y\ln^{l_2}(f)f^{-k_2/3}) = (h^Y|h^Y\ln^{l_1+l_2}(f)f^{-(k_1+k_2)/3}) = \mathrm{A}^2I(k_1+k_2+7,l_1+l_2)^Y$.

The detector PSD moments required for the metric calculation associated with restricted SPA TaylorF2 inspiral waveforms expanded to 3.5 PN order are

$$(k,l)\in\{(1,0),(2,0),(3,0),(4,0),(5,0),(6,0),$$
$$(7,0),(8,0),(9,0),(10,0),(11,0),$$
$$(12,0),(13,0),(14,0),(15,0),(17,0),$$
$$(3,1),(4,1),(5,1),(6,1),(7,1),(8,1),$$
$$(9,1),(10,1),(11,1),(12,1),$$
$$(5,2),(6,2),(7,2)\}.$$

APPENDIX F: DERIVATIVES OF PN COEFFICIENTS

Here we give explicit expressions for the derivatives of the PN coefficients associated with the phase in terms of the symmetric mass ratio η and the chirp mass $\mathcal{M}$, as computed in [9]. First, the derivatives with respect to $\mathcal{M}$ are

$$\partial_{\mathcal{M}}\psi_0 = \frac{-5}{128\pi^{5/3}\mathcal{M}^{8/3}}, \quad \text{(F1)}$$

$$\partial_{\mathcal{M}}\psi_2 = \frac{-5}{384\pi\mathcal{M}^2\eta^{2/5}}\Big(\frac{743}{84}+11\eta\Big), \quad \text{(F2)}$$

$$\partial_{\mathcal{M}}\psi_3 = \frac{\pi^{1/3}}{4\mathcal{M}^{5/3}\eta^{3/5}}, \quad \text{(F3)}$$

$$\partial_{\mathcal{M}}\psi_4 = \frac{-5}{9216\pi^{1/3}\mathcal{M}^{4/3}\eta^{4/5}} \times\left(\frac{3058673}{7056}+\frac{5429}{7}\eta+617\eta^2\right), \quad \text{(F4)}$$

$$\partial_{\mathcal{M}}\psi_5 = \frac{5\pi}{384\mathcal{M}\eta}\left(\frac{7729}{84}-13\eta\right), \quad \text{(F5)}$$

$$\partial_{\mathcal{M}}\psi_6 = \frac{\pi^{1/3}}{384\mathcal{M}^{2/3}\eta^{6/5}}\left(\frac{10052469856691}{1564738560}-640\pi^2 - \frac{6848}{7}[\gamma+\ln(4\pi^{1/3}\mathcal{M}^{1/3}\eta^{-1/5})] + \frac{5}{4}\left[\frac{-3147553127}{254016}+451\pi^2\right]\eta + \frac{76055}{576}\eta^2-\frac{127825}{432}\eta^3\right), \quad \text{(F6)}$$

$$\partial_{\mathcal{M}}\psi_6^l = \frac{-107\pi^{1/3}}{126\mathcal{M}^{2/3}\eta^{6/5}}, \quad \text{(F7)}$$

$$\partial_{\mathcal{M}}\psi_7 = \frac{5\pi^{5/3}}{48384\mathcal{M}^{1/3}\eta^{7/5}} \times\left(\frac{15419335}{336}+\frac{75703}{2}\eta-14809\eta^2\right). \quad \text{(F8)}$$

Now the derivatives with respect to η are

$$\partial_\eta\psi_2 = \frac{-1}{384\pi\mathcal{M}\eta^{7/5}}\left(\frac{743}{42}-33\eta\right), \quad \text{(F9)}$$

$$\partial_\eta\psi_3 = \frac{9\pi^{1/3}}{40\mathcal{M}^{2/3}\eta^{8/5}}, \quad \text{(F10)}$$

$$\partial_\eta\psi_4 = \frac{-3}{3072\pi^{1/3}\mathcal{M}^{1/3}\eta^{9/5}} \times\left(\frac{3058673}{5292}-\frac{5429}{21}\eta+1234\eta^2\right), \quad \text{(F11)}$$

$$\partial_\eta\psi_5 = \frac{-\pi}{384\eta^2}\times\left(\frac{7729}{84}[8+5\ln(6^{3/2}\pi\mathcal{M}\eta^{-3/5})]-39\eta\right), \quad \text{(F12)}$$

$$\partial_\eta\psi_5^l = \frac{-38645\pi}{32256\eta^2}, \quad \text{(F13)}$$

$$\partial_\eta\psi_6 = \frac{-\pi^{1/3}\mathcal{M}^{1/3}}{640\eta^{11/5}}\left(\frac{11328104339891}{260789760} - 3840\pi^2-\frac{41088}{7}[\gamma+\ln(4\pi^{1/3}\mathcal{M}^{1/3}\eta^{-1/5})] + \frac{5}{4}\left[\frac{-3147553127}{254016}+451\pi^2\right]\eta - \frac{76055}{144}\eta^2+\frac{127825}{48}\eta^3\right), \quad \text{(F14)}$$

$$\partial_\eta\psi_6^l = \frac{107\pi^{1/3}\mathcal{M}^{1/3}}{35\eta^{11/5}}, \quad \text{(F15)}$$

$$\partial_\eta\psi_7 = \frac{-\pi^{5/3}\mathcal{M}^{2/3}}{32256\eta^{12/5}} \times\left(\frac{15419335}{48}+75703\eta+44427\eta^2\right). \quad \text{(F16)}$$

Any derivatives of the coefficients of 3.5 PN order or lower not defined above are identically zero.

The phase also contains a term associated with the relative time shift between the arrival of a signal at a detector's location compared to the arrival of the signal at the geocenter. These derivatives are as follows:

$$\partial_\alpha t^Y = -\frac{\vec{r}_Y\cdot\partial_\alpha\hat{n}}{c}, \quad \text{(F17a)}$$

$$\partial_\delta t^Y = -\frac{\vec{r}_Y\cdot\partial_\delta\hat{n}}{c}, \quad \text{(F17b)}$$

where $\partial_\alpha\hat{n}$ and $\partial_\delta\hat{n}$ are given by (B3a) and (B3b), respectively.

[1] LIGO Scientific Collaboration, Virgo Collaboration, and K. Belczynski, Class. Quantum Grav. **27**, 173001 (2010).
[2] S. Bose, A. Pai, and S. Dhurandhar, Int. J. Mod. Phys. D **09**, 325 (2000).
[3] L. S. Finn, Phys. Rev. D **63**, 102001 (2001).
[4] C. Cutler and B. F. Schutz, Phys. Rev. D **72**, 063006 (2005).
[5] I. W. Harry and S. Fairhurst, Phys. Rev. D **83**, 084002 (2011).
[6] P. Jaranowski, A. Królak, and B. F. Schutz, Phys. Rev. D **58**, 063001 (1998).
[7] B. J. Owen, Phys. Rev. D **53**, 6749 (1996).
[8] B. J. Owen and B. S. Sathyaprakash, Phys. Rev. D **60**, 022002 (1999).
[9] D. Keppel, A. Lundgren, B. J. Owen, and H. Zhu, Technical Report P12001652 (LIGO Scientific Collaboration, 2012).
[10] D. H. Brown, I. Harry, A. Lundgren, and A. A. Nitz, Phys. Rev. D **86**, 084017 (2012).

[11] A. Pai, S. Dhurandhar, and S. Bose, Phys. Rev. D **64**, 042004 (2001).
[12] A. Pai, S. Bose, and S. Dhurandhar, Class. Quantum Grav. **19**, 1477 (2002).
[13] R. Prix, Phys. Rev. D **75**, 023004 (2007).
[14] L. Wen and Y. Chen, Phys. Rev. D **81**, 082001 (2010).
[15] P. Ajith and S. Bose, Phys. Rev. D **79**, 084032 (2009).
[16] J. Abadie, B. P. Abbott, R. Abbott, T. D. Abbott, M. Abernathy, T. Accadia, F. Acernese, C. Adams, R. Adhikari *et al.* (LIGO Scientific Collaboration and Virgo Collaboration), Astrophys. J. **760**, 12 (2012).
[17] V. Predoi (for the LIGO Scientific Collaboration and Virgo Collaboration) and K. Hurley (for the IPN), J. Phys. Conf. Ser. **363**, 012034 (2012).
[18] S. Bose, T. Dayanga, S. Ghosh, and D. Talukder, Class. Quantum Grav. **28**, 134009 (2011).
[19] R. Prix, Technical Report No. T0900149-v4, LIGO Scientific Collaboration, 2012.
[20] M. Rakhmanov, J. D. Romano, and J. T. Whelan, Class. Quantum Grav. **25**, 184017 (2008).
[21] A. Królak, M. Tinto, and M. Vallisneri, Phys. Rev. D **70**, 022003 (2004).
[22] P. Jaranowski and A. Królak, Living Rev. Relativity **15**, 4 (2012).
[23] LIGO Scientific Collaboration, Technical Report T0900288-v2 (LIGO Scientific Collaboration, 2009).
[24] Virgo Scientific Collaboration (2010).
[25] T. Damour, B. R. Iyer, and B. S. Sathyaprakash, Phys. Rev. D **63**, 044023 (2001).
[26] A. Buonanno, B. R. Iyer, E. Ochsner, Y. Pan, and B. S. Sathyaprakash, Phys. Rev. D **80**, 084043 (2009).
[27] S. Fairhurst, New J. Phys. **11**, 123006 (2009).
[28] S. Fairhurst, Class. Quantum Grav. **28**, 105021 (2011).
[29] S. Fairhurst, arXiv:1205.6611.
[30] A. Klöckner, N. Pinto, Y. Lee, B. Catanzaro, P. Ivanov, and A. Fasih, arXiv:0911.3456.